10th World Congress on Structural and Multidisciplinary Optimization
May 19 -24, 2013, Orlando, Florida, USA

Optimization of Variable Blank Holder Force Trajectory via Sequential Approximate Optimization with Radial Basis Function network

Satoshi Kitayama[1], Kenta Kita[2], Koetsu Yamazaki[3]

[1] Kanazawa University, Kanazawa, Japan, kitagon@t.kanazawa-u.ac.jp
[2] Toshiba Corporation, Tokyo, Japan
[3]Kanazawa University, Kanazawa, Japan, yamazaki@t.kanazawa-u.ac.jp

1. Abstract
This paper proposed sequential approximate optimization (SAO) with radial basis function (RBF) network. In the SAO, the sampling strategy is one of the important issues. The RBF network is used throughout the proposed SAO. In order to find the unexplored region, new function called the density function is constructed. By minimizing the density function, new sampling points are added around the unexplored region. The proposed SAO is applied to the optimization of the variable blank holder force trajectory in deep drawing.
2. Keywords: Sequential Approximate Optimization, Radial Basis Function network, Sheet Forming, Variable Blank Holder Force Trajectory

3. Introduction
In sheet forming, there are many factors that affect the quality of products, such as the Blank Holder Force (BHF), the friction and lubrication conditions of the interface, and the die geometry. Among these factors, BHF plays a key role in sheet forming. In most cases, a constant BHF is applied over the punch stroke. A lower BHF will cause wrinkling due to excessive material flow into the die, while a higher BHF will lead to tearing due to the thinning. Wang et al. [1] suggested that there are four basic windows for BHF formability, as shown in Fig.1. These formability windows represent the relationship between the BHF and the punch stroke.

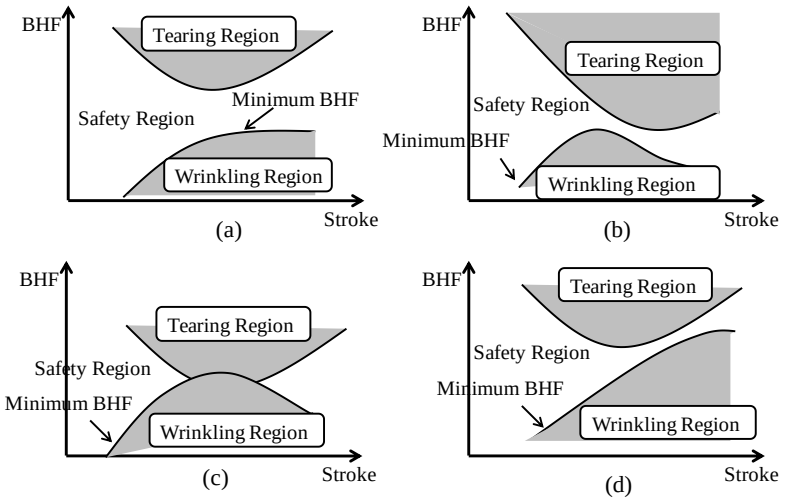

Fig.1 Four basic BHF formability windows

In the formability windows shown in Fig.1(a), it is possible to form a sheet without wrinkling and tearing with an appropriate constant BHF. It is impossible, however, to form a sheet with a constant BHF in other cases. In the formability windows shown in Figs.1(b), and (c), particularly, the Variable Blank Holder Force (VBHF) approach, in which the BHF varies throughout the stroke, is preferable. The formability windows shown in Fig.1 are unknown, so that CAE with optimization techniques is a powerful tool. Numerous researches have been conducted on the VBHF and VBHF trajectory with CAE and optimization techniques. They can be roughly classified into two categories: One is based on the closed-loop type algorithms [2-4], and the other is based on the response surface methodologies (RSM) [5-7]. VBHF trajectory with the closed-loop type algorithms is not formulated as a mathematical optimization problem. Brief reviews on the closed-loop type algorithms can be found in Ref.[2]. In contrast to the closed-loop type algorithms, RSM is one of the optimization approaches. We mainly focus on the RSM approach for VBHF trajectory.

Here, some issues to apply RSM to sheet forming are summarized as bellow:
(P1) In RSM approach, the forming limit diagram (FLD) is widely and commonly employed to evaluate the risk of both wrinkling and tearing. The risk of both wrinkling and tearing are handled as one of the objectives. In some of researches, the risk of tearing can be handled as the objective function. As the suggestion by Jakumeit et al. [8], it is natural to handle the risk of both wrinkling and tearing as the constraint. In addition, we consider that wrinkling and tearing should be evaluated separately.
(P2) In order to construct the response surface, the most of the researches employ the quadratic polynomial as the response surface [9-11]. In general, sheet forming is highly non-linear phenomena, and the Gaussian-based RSM such as Kriging and Radial Basis Function (RBF) network should be used.
(P3) In general, sheet forming simulation is a time-consuming task. Considering the application of the optimization technique in industries, the RSM is a preferable and practical approach. Nowadays, SAO is widely studied. In SAO, the response surface is constructed repeatedly by adding new sampling points. One of the important topics in SAO is the sampling strategy.
In this paper, an optimal VBHF trajectory by SAO with the RBF network is determined. The objective function is to minimize the thickness deviation between the initial and the final state of the blank. The risk of both wrinkling and tearing is evaluated with the FLD. In addition, the risk of wrinkling and tearing is evaluated separately. Therefore, the optimization problem considered here has two constraints. The BHF is partitioned through the punch stroke, and the BHFs are taken as the design variables. The RBF network is employed to construct the response surface. In SAO, global and local approximations will be achieved simultaneously through the sequential sampling strategy. For local approximation, an optimum of response surface is added as the new sampling point. For global approximation, several new sampling points are added around the unexplored region. In order to find the unexplored region, a new function which is called the density function is developed with the RBF network. The algorithm of the proposed SAO is proposed. The proposed SAO is applied to determine the VBHF trajectory. LS-DYNA, which is one of the dynamic explicit Finite Element Analysis (FEA) codes, is employed in the numerical simulation.

4. Sequential Approximate Optimization with Radial Basis Function network

In this paper, RBF network is used throughout the SAO procedure. First, RBF network is briefly described. Secondly, new function called the density function is explained. An illustrative example is given for the better understanding.

4.1. Radial Basis Function network

The RBF network is a three-layer feed-forward network. The output of the network $f_a(\boldsymbol{x})$, which corresponds to the response surface, is given by

$$f_a(\boldsymbol{x}) = \sum_{i=1}^{m} w_i h_i(\boldsymbol{x}) \tag{1}$$

where m represents the number of sampling points, $h_i(\boldsymbol{x})$ is the i-th basis function, and w_i denotes the weight of the i-th basis function. In this paper, the following Gaussian kernel is used as the basis function.

$$h_i(\boldsymbol{x}) = \exp\left(-\frac{(\boldsymbol{x}-\boldsymbol{x}_i)^T(\boldsymbol{x}-\boldsymbol{x}_i)}{r_i^2}\right) \tag{2}$$

In Eq(2), $\boldsymbol{x}_i$ represents the i-th sampling point, and r_i is the width of the i-th basis function. The response y_i is calculated at sampling point $\boldsymbol{x}_i$. The learning of the RBF network is usually accomplished by solving the following equation:

$$E = \sum_{i=1}^{m} (y_i - f_a(\boldsymbol{x}_i))^2 + \sum_{i=1}^{m} \lambda_i w_i^2 \rightarrow \min \tag{3}$$

where the second term is introduced for the purpose of regularization. It is recommended that λ_i in Eq.(3) have a sufficiently small value (e.g. $\lambda_i = 1.0\times10^{-3}$). Thus, the learning of the RBF network is equivalent to finding the weight vector $\boldsymbol{w}$. The necessary condition of Eq.(3) leads to the following equation:

$$\boldsymbol{w} = (\boldsymbol{H}^T\boldsymbol{H} + \boldsymbol{\Lambda})^{-1}\boldsymbol{H}^T\boldsymbol{y} \tag{4}$$

where $\boldsymbol{H}$, $\boldsymbol{\Lambda}$, and $\boldsymbol{y}$ are given as follows:

$$\boldsymbol{H} = \begin{bmatrix} h_1(\boldsymbol{x}_1) & h_2(\boldsymbol{x}_1) & \cdots & h_m(\boldsymbol{x}_1) \\ h_1(\boldsymbol{x}_2) & h_2(\boldsymbol{x}_2) & \cdots & h_m(\boldsymbol{x}_2) \\ \vdots & \vdots & \ddots & \vdots \\ h_1(\boldsymbol{x}_m) & h_2(\boldsymbol{x}_m) & \cdots & h_m(\boldsymbol{x}_m) \end{bmatrix} \tag{5}$$

$$\boldsymbol{\Lambda} = \begin{bmatrix} \lambda_1 & 0 & \cdots & 0 \\ 0 & \lambda_2 & \cdots & 0 \\ \vdots & \vdots & \ddots & \vdots \\ 0 & 0 & 0 & \lambda_m \end{bmatrix} \tag{6}$$

$$\boldsymbol{y} = (y_1, y_2, \cdots, y_m)^T \tag{7}$$

It is clear from Eq.(4) that the learning of the RBF network is equivalent to the matrix inversion $(\boldsymbol{H}^T\boldsymbol{H} + \boldsymbol{\Lambda})^{-1}$. It is easy to calculate the weight vector $\boldsymbol{w}$, because the additional learning is reduced to the incremental calculation of the matrix inversion.

4.2. Width in Gaussian kernel

The width in the Gaussian kernel plays an important role for good approximation. Nakayama proposed the following simple estimate of width [12]:

$$r = \frac{d_{\max}}{\sqrt[n]{nm}} \tag{8}$$

where n denotes the number of design variables, m denote the number of sampling points, and $d_{\max}$ denotes the maximum distance between sampling points. Eq.(8) is equally applied to all Gaussian kernel, thus, $r_1=r_2=\ldots=r_m=r$. This equation may work well in the case of uniform distribution of the sampling points. However, most real engineering problems show non-uniform distribution of the sampling points. We have examined Eq.(8), and have proposed the following simple estimate [13]:

$$r_j = \frac{d_{j,\max}}{\sqrt{n}\sqrt[n]{m-1}} \quad j = 1, 2, \cdots, m \tag{9}$$

where $d_{j,\max}$ denotes the maximum distance between the j-th sampling point and another one in the sampling points. Eq.(9) is applied to each Gaussian kernel individually unlike Eq.(8). In Eq.(8), $d_{\max}$ is always constant in both the uniform and non-uniform distribution of the sampling points. This implies that non-uniform distribution of the sampling points cannot be taken into account. In contrast, $d_{j,\max}$ is employed in Eq.(9), and non-uniform distribution of the sampling points can be taken into account.

4.3 Density Function

In the SAO, it is important to find out the unexplored region for global approximation. The Kriging can achieve this objective with the expected improvement (EI) function. In order to find out the unexplored region with the RBF network, we have developed a function called the density function [13]. The basic idea is very simple. The local maxima are generated at the sampling points. To achieve this objective, every output $\boldsymbol{y}$ of the RBF network is replaced with +1. The procedure to construct the density function is summarized as follows:

(D-STEP1) The following vector $\boldsymbol{y}^D = (1,1,\cdots,1)^T_{m\times 1}$ is prepared at the sampling points.

(D-STEP2) The weight vector $\boldsymbol{w}^D$ of the density function $D(\boldsymbol{x})$ is calculated as follows:

$$\boldsymbol{w}^D = (\boldsymbol{H}^T\boldsymbol{H} + \boldsymbol{\Lambda})^{-1}\boldsymbol{H}^T\boldsymbol{y}^D \tag{10}$$

(D-STEP3) The density function $D(\boldsymbol{x})$ is minimized, and the point minimizing $D(\boldsymbol{x})$ is taken as the new sampling point.

$$D(\boldsymbol{x}) = \sum_{j=1}^{m} w_j^D h_j(\boldsymbol{x}) \to \min \tag{11}$$

Figure 2 shows an illustrative example in one dimension. The black dots denote the sampling points. It is found from Fig.2 that local minima are generated around the unexplored region.

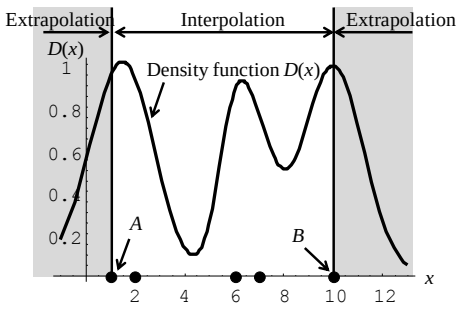

Fig.2 Illustrative example of density function in one dimension

4.4 Algorithm of SAO with RBF network

Figure 3 shows the detailed algorithm for SAO with the RBF network. In this paper, the terminal criterion of SAO is determined by the maximum number of sampling points, m_{max}.

The proposed SAO algorithm is roughly divided into two phases. The first phase is used to construct the response surface and add the optimum of response surface as a new sampling point. Thus, in the first phase, the number of new sampling points is one that is the optimum of the response surface. The second phase is used to construct the density function and add the optimum of the density function as a new sampling point. It should be noted that the density function is constructed until the terminal criterion, which is described later, is satisfied. As a result, many new sampling points will be added, according to the number of design variables, n .

Let us consider the first phase. First, the initial sampling points are determined by using the orthogonal array, the Latin hypercube design (LHD), and so on. Assume that the number of sampling points is m. The RBF network is employed to construct the response surface from m sampling points, and we find the optimum of the response surface. The optimum of the response surface is directly taken as the new sampling point. In this phase, the number of sampling points is updated as $m = m + 1$.

Then, the second phase, in which the density function is constructed, is considered. The density function is also constructed by the RBF network. The optimum of the density function is taken as the new sampling point, and the number of sampling points is updated as shown in Fig.3. As show in Fig.3, the parameter *count* is introduced in this phase. This parameter controls the number of sampling points that can be obtained by the density function. Thus, in the proposed algorithm, the number of sampling points by the density function varies according to the number of design variables. If the parameter *count* is less than int(n/2), this parameter is increased as *count* = *count* +1. The terminal criterion in the second phase is given by int(n/2), where int() represents the rounding-off. If the terminal criterion is satisfied, the number of sampling point m is compared with m_{max}. If the m is less than m_{max}, the objective function and constraints are calculated as shown in Fig.5. Otherwise, the algorithm is terminated.

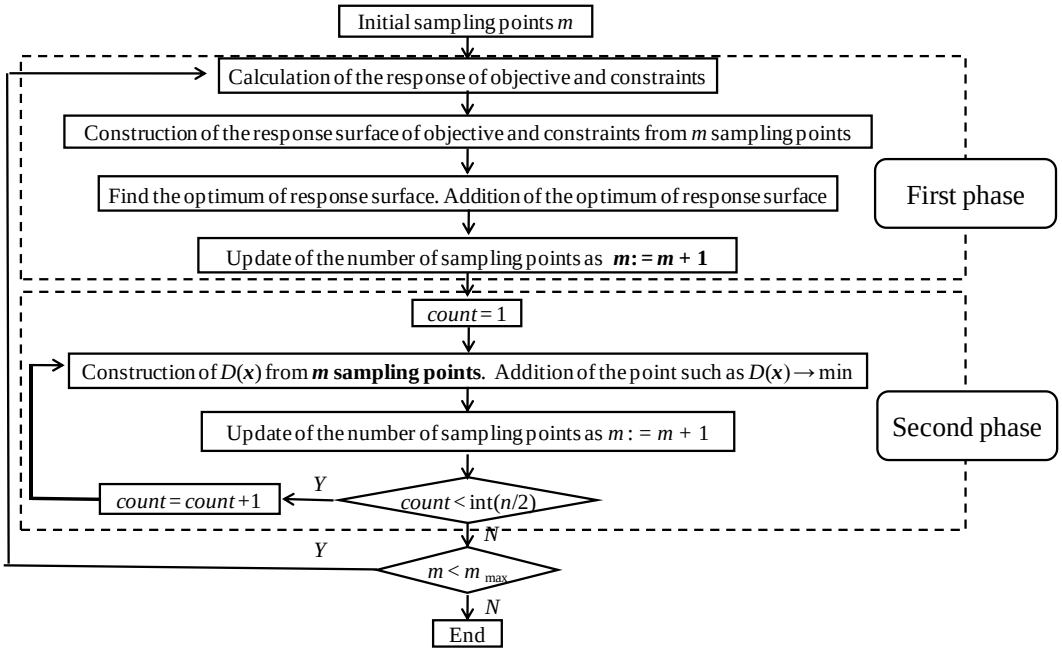

Fig.3 Proposed SAO algorithm

5. Optimization of Variable Blank Holder Force Trajectory in Deep Drawing

The proposed SAO algorithm with RBF network is applied to the optimization of the variable blank holder force trajectory in deep drawing. First, the Finite Element Analysis (FEA) model is described. Secondly, the design optimization problem is formulated.

5.1 Finite Element Analysis model

An experimental test was performed with a constant BHF (=100 kN). SPFC440 (Steel Plate Formability Cold) was selected as the test material for which the material properties are shown in Table 1. The material properties shown in Table 1 are obtained through the experiment. In the experiment, the total length of stroke L_{max} is 62 mm. The stress-strain relationship is defined as follows:

$$\sigma = 793\varepsilon^{0.189} \tag{12}$$

The blank size is 185 x 185mm, and the initial thickness is 1.20 mm. The square cup deep drawn part obtained in

the experiment is shown in Fig.4(a), and its dimensions are shown in Fig.4(b). In this case, no wrinkling or tearing can be observed.

Table 1 Material properties of SPFC440

Density: ρ [kg/mm^3]	7.84×10^{-6}
Young's Modulus: E [MPa]	2.06×10^{5}
Poisson's Ratio: ν	0.3
Yield Stress: σ_Y [MPa]	353
Tensile Strength: σ_T [MPa]	479
Normal Anisotropy Coefficient: r	0.98
Strain Hardening Coefficient: n	0.189

Fig.4(a) Molding in experiment

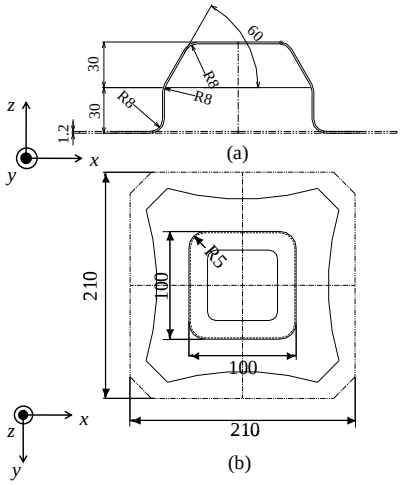

Fig.4(b) Dimensions of molding

All numerical simulations are performed with LS-DYNA. Considering the geometrical and material symmetry, one fourth model is employed in the numerical simulation, as shown in Fig.5. The element type and the number of finite elements are shown in Table 2. A constant friction coefficient μ of 0.10 is used for all contact surfaces. The penalty coefficient for contact is set to 0.10.

Table 2 Element type and number of finite elements

	Element type	Number of finite elements
Counter punch	Rigid	120
Die	Rigid	924
Blank	Shell (Belytschko-Tsay)	2116
Blank holder	Rigid	432
Punch	Rigid	962

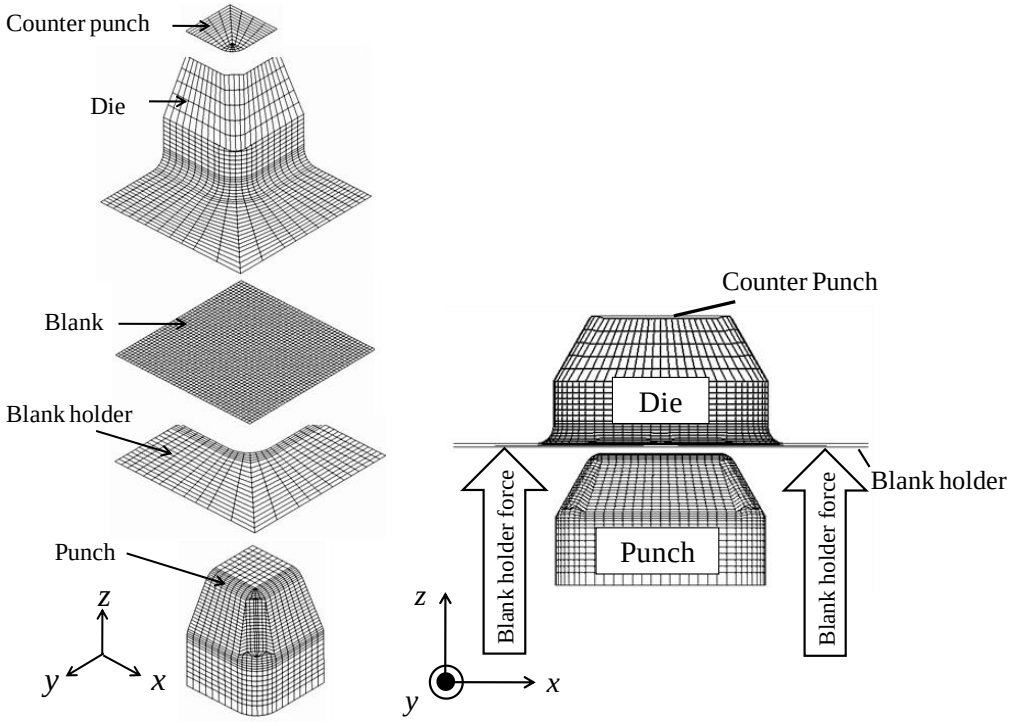

Fig.5 Finite element models

5.2 Design Variables

Total stroke $L_{\max}$ is partitioned into n stroke. The BHF of the each stroke step is taken as the design variables. An illustrative example of the design variables are shown in Fig.6.

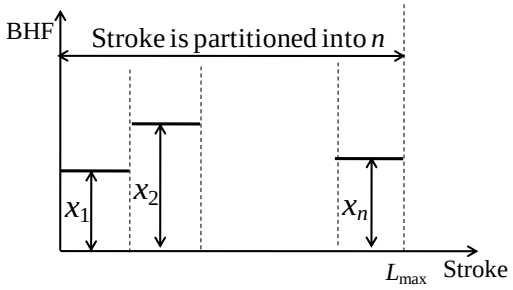

Fig.6 Design variables

5.3 Objective Function

In deep drawing, the maximum thinning can be observed at the corner parts of the punch, and will lead to tearing. In order to prevent the tearing, it is considered that the minimization of the maximum thinning of the blank may be valid. However, we cannot consider the thickness deviation of whole blank. According to Refs. [10, 11], the thickness deviation by Eq. (13) is taken as the objective function.

$$(\sum_{i=1}^{nelm}(t_i/t_0-1)^p)^{1/p} \rightarrow \min \tag{13}$$

where *nelm* denotes the number of finite elements of the blank, t_i denotes the final thickness of the *i*-th element, t_0 denotes the initial thickness, and coefficient $p=2,4,6,\cdots$ is the parameter to emphasize the extreme of Eq.(13). According to Ref.[11], p is set to 4.

5.4 Design Constraints

Many researches handle the risk of both wrinkling and tearing as the objective [6, 8, 10, 11]. In this paper, the risk of both wrinkling and tearing is handled as the constraints, separately. Let us consider the FLD as shown in Fig.7. In order to evaluate the risk of both wrinkling and tearing, the strains in the formed element are analyzed and compared against the forming limit curve (FLC, as shown in Fig.7). We define the following FLC in the principal plan of logarithmic strains proposed by Hillman and Kubli [14].

$$\varepsilon_1=\varphi_T(\varepsilon_2),\ \varepsilon_1=\varphi_W(\varepsilon_2) \tag{14}$$

where φ_T is the FLC which controls tearing, and φ_W is also the FLC which controls wrinkling. Both of them depend on the material; they are generally given as knots data in tables. Then, the following safety FLC is defined:

$$\theta_T(\varepsilon_2) = (1-s)\varphi_T(\varepsilon_2) \tag{15}$$

$$\theta_W(\varepsilon_2) = (1+s)\varphi_W(\varepsilon_2) \tag{16}$$

where *s* represents the safety tolerance, and is defined by the engineers. If an element comes to or lies above FLC, it is expected that a risk of tearing can be observed. Similarly, a risk of wrinkling can be assumed if an element lies in the wrinkling region.

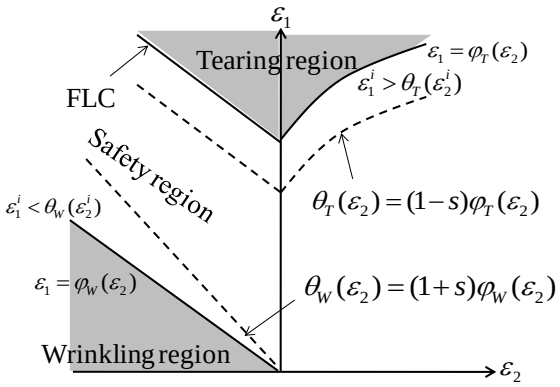

Fig.7 Forming Limit Diagram (FLD)

In order to clarify which risks are evaluated, we separately evaluate the risk of both wrinkling and tearing. In this paper, the following two constraints are formulated:
For tearing:

$$g_1(\boldsymbol{x}) = (\sum_{j=1}^{nelm} T_j)^{1/p} \tag{17}$$

where

$$\begin{aligned} T_j &= (\varepsilon_1^j - \theta_T(\varepsilon_2^j))^p \quad \varepsilon_1^j > \theta_T(\varepsilon_2^j) \\ T_j &= 0 \qquad\qquad \textit{otherwise} \end{aligned} \tag{18}$$

For wrinkling:

$$g_2(\boldsymbol{x}) = (\sum_{j=1}^{nelm} W_j)^{1/p} \tag{19}$$

where

$$\begin{aligned} W_j &= (\theta_W(\varepsilon_2^j) - \varepsilon_1^j)^p \quad \varepsilon_1^j < \theta_W(\varepsilon_2^j) \\ W_j &= 0 \qquad\qquad \textit{otherwise} \end{aligned} \tag{20}$$

Like the objective function, *p* is set to 4.

6. Numerical Simulation

The lower and upper bounds on the design variables are set to 20 kN and 150 kN, respectively. The total stroke is partitioned into six as follows:

$$\left.\begin{aligned} 0.00 \le L_1 \le 10.09 \quad 10.09 \le L_2 \le 21.07 \quad 21.07 \le L_3 \le 31.93 \\ 31.93 \le L_4 \le 41.61 \quad 41.61 \le L_5 \le 51.50 \quad 51.50 \le L_6 \le 62.00 \end{aligned}\right\} \tag{21}$$

Fifteen initial sampling points are determined with the LHD. The proposed SAO algorithm will be terminated at thirty sampling points. The final VBHF trajectory with the proposed SAO algorithm is shown in Fig. 8 with the forming process. In order to evaluate the wrinkling and the tearing, the safety tolerance *s* in Eqs. (15) and (16) should be set. Two different safety tolerances are employed in numerical simulation. In Fig.8, the solid line is VBHF trajectory with *s*=0.1, and the dashed line is the one with *s*=0.2.
It is clear from Fig.8 that the safety tolerance has little effect on the optimal VBHF trajectories. BHF drops down at 10.09 mm, and gradually rises up as the punch stroke proceeds. It is noteworthy that lower BHF is applied to the blank during the corner parts forming for preventing tearing, while higher BHF is applied after the corner parts have been formed for preventing wrinkling. The thickness distributions by two optimal VBHF trajectories are shown in Fig. 9, and the FLD with *s*=0.2 is also shown in Fig.10.

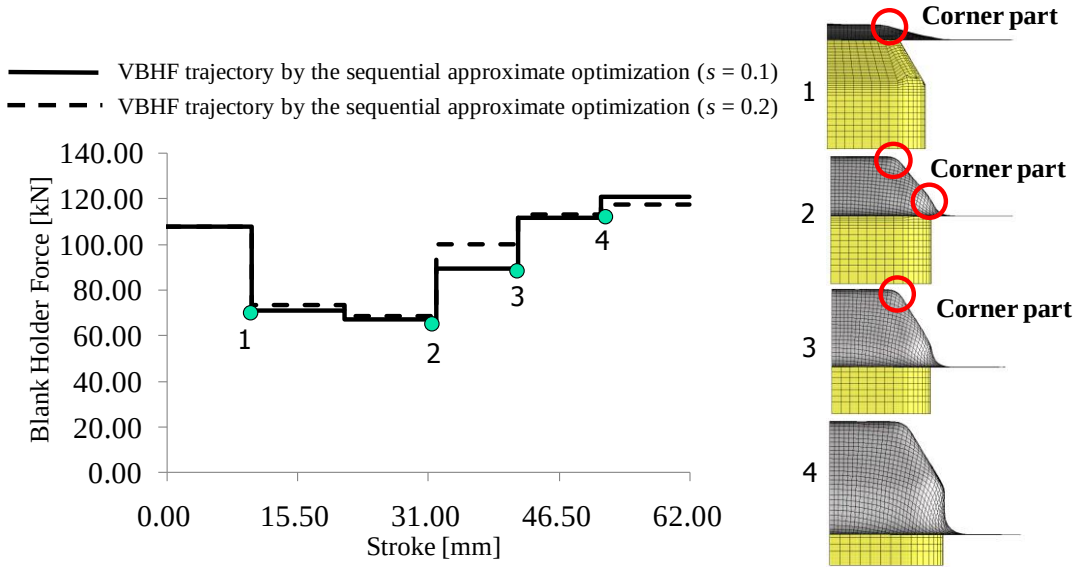

Fig. 8 Optimal VBHF trajectories with different safety tolerance

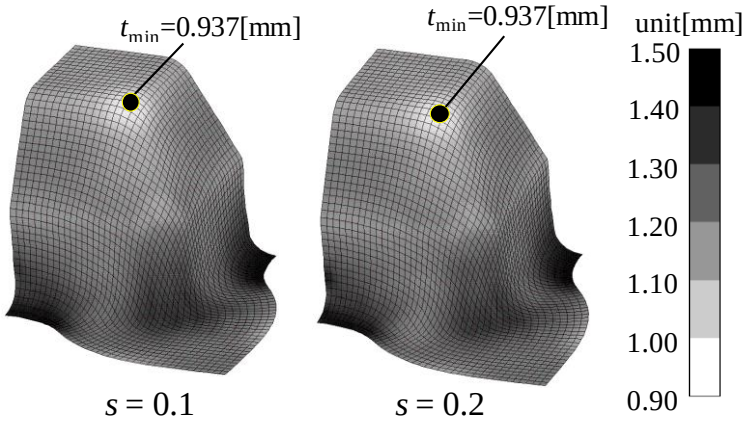

Fig.9 Thickness distributions by optimal VBHF trajectories

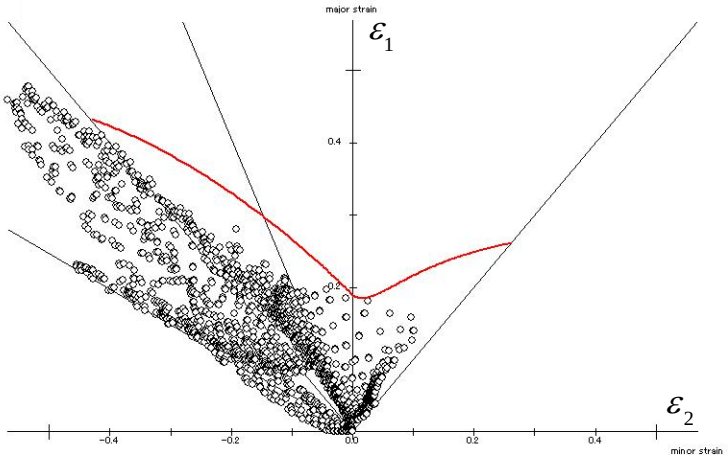

Fig.10 Forming Limit Diagram of the VBHF trajectory (s=0.2)

The errors at the optimal solution between response surface and numerical simulation are listed in Table 3. It is clear from Table 3 that $g_1(\boldsymbol{x})$ (tearing) is more active than $g_2(\boldsymbol{x})$ (wrinkling). This implies that tearing is more important constraint than wrinkling at the optimum solution. In industries, tearing directly leads to defective piece, and then tearing is more undesirable issue than wrinkling. Therefore, tearing is more important than wrinkling.

This optimization result is consistent with the comments of experts in industries.

Table 3 Errors between response surface and numerical simulation

	s	$f(\boldsymbol{x})$	$g_1(\boldsymbol{x})$ (Tearing)	$g_2(\boldsymbol{x})$ (Wrinkling)
Reponse Surface	0.1	6.29E-01	7.68E-03	6.24E-02
	0.2	6.40E-01	3.55E-02	1.00E-01
Numerical Simulation	0.1	6.12E-01	7.80E-03	6.34E-02
	0.2	5.97E-01	3.50E-02	1.02E-01
Error [%]	0.1	2.86	1.53	1.49
	0.2	7.09	1.43	1.84

7. Conclusion

In this paper, the sequential approximate optimization procedure with the RBF network is employed to find the optimal variable blank holder force trajectory. In the SAO, the sampling strategy is one of the important issues. In this paper, the density function with the RBF network to find the unexplored region is developed. By minimizing the density function, new sampling points are added around the unexplored region. The RBF network is used throughout the proposed SAO procedure.

The proposed SAO was applied to the optimal VBHF trajectory of square cup deep drawing. In particular, the risk of both tearing and wrinkling is separately handled as the constraints. It is noteworthy that lower BHF is applied to the blank during the corner parts forming for preventing tearing, while higher BHF is applied after the corner parts have been formed for preventing wrinkling. Through numerical simulation, no tearing and wrinkling can be observed. It can be found from optimization result that tearing is more evaluated than wrinkling at the optimum solution. In industries, tearing directly leads to defective piece, and then tearing is more undesirable issue than wrinkling. Therefore, tearing is more important than wrinkling. This optimization result was consistent with the comments of experts in industries.

8. References

[1] Wang, W.R., Chen, G.L., Lin, Z.Q., Li, S.H., (2007), Determination of optimal blank holder force trajectories for segmented binders of step rectangle box using PID closed-loop FEM simulation, *International Journal of Advanced Manufacturing Technology*, 32: 1074-1082

[2] Kitayama, S., Hamano, S., Yamazaki, K., Kubo, T., Nishikawa, H., Kinoshita, H., (2010), A closed-loop type algorithm for determination of variable blank holder force trajectory and its application to square cup deep drawing, *International Journal of Advanced Manufacturing Technology*, 51: 507-571

[3] Lin, Z.Q., Wang, W.R., Chen, G.L. (2007), A new strategy to optimize variable blank holder force towards improving the forming limits of aluminum sheet metal forming, *Journal of Materials Processing Technology*, 183: 339-346

[4] Sheng, Z.Q., Jirathearanat, S., Altan, T., (2004), Adaptive FEM simulation for prediction of variable blank holder force in conical cup drawing, *Journal of Machine Tools and Manufacturing*, 44: 487-494.

[5] Jansson, T., Nilsson, L., Redhe, M., (2003), Using surrogate models and response surface in structural optimization -with application to crashworthiness design and sheet metal forming, *Structural and Multidisciplinary Optimization*, 25: 129-140

[6] Chengzhi, S., Guanlong, C., Zhongqin, L., (2005), Determining the optimum variable blank-holder forces using adaptive response surface methodology (ARSM), *International Journal of Advanced Manufacturing Technology*, 26: 23-29

[7] Wang, H., Li, G.Y., Zhong, Z.H., (2008), Optimization of sheet metal forming processes by adaptive response surface based on intelligent sampling method, *Journal of Materials Processing Technology*, 197: 77-88

[8] Jakumeit, J., Herdy, M., Nitsche, M., (2005), Parameter optimization of the sheet metal forming process using an iterative parallel Kriging algorithm, *Structural and Multidisciplinary Optimization*, 29: 498-507

[9] Naceur, H., Ben-Elechi, S., Batoz, J.L., Knopf-Lenoir C., (2008), Response surface methodology for the rapid design of aluminum sheet metal forming parameters, *Materials and Design*, 29: 781-790

[10] Breitkopf, P., Naceur, H., Rassineux, A., Villon, P., (2005), Moving least squares response surface approximation: Formulation and metal forming applications, *Computers and Structures*, 83: 1411-1428

[11] Wang, H., Li, E., Li, G.Y., (2008), Optimization of drawbead design in sheet metal forming based on intelligent sampling by using response surface methodology, *Journal of Materials Processing Technology*, 206: 45-55

[12] Nakayama, H., Arakawa, M., Sasaki, R., (2002), Simulation-based optimization using computational

intelligence, *Optimization and Engineering*, 3: 201-214.
[13] Kitayama, S., Arakawa, M., Yamazaki, K., (2011), Sequential approximate optimization using radial basis function network for engineering optimization, *Optimization and Engineering*, 12 (4): 535-557.
[14] Hillmann,M., Kubli, W., (1999) Optimization of sheet metal forming processes using simulation programs, *In: Numisheet 99*, Beasnc, France, Vol.1 287-292.